Research Article Vol. 5, No. 11 / November 2018 / Optica 1455

Quantum interference and correlation control of frequency-bin qubits

Hsuan-Hao Lu,[1,†] Joseph M. Lukens,[2,†,*] Nicholas A. Peters,[2,3] Brian P. Williams,[2] Andrew M. Weiner,[1] and Pavel Lougovski[2,4]

[1]School of Electrical and Computer Engineering and Purdue Quantum Center, Purdue University, West Lafayette, Indiana 47907, USA
[2]Quantum Information Science Group, Computational Sciences and Engineering Division, Oak Ridge National Laboratory, Oak Ridge, Tennessee 37831, USA
[3]Bredesen Center for Interdisciplinary Research and Graduate Education, University of Tennessee, Knoxville, Tennessee 37996, USA
[4]e-mail: lougovskip@ornl.gov
*Corresponding author: lukensjm@ornl.gov

Received 12 July 2018; revised 18 October 2018; accepted 19 October 2018 (Doc. ID 338659); published 9 November 2018

Frequency-bin quantum information encoding offers an intriguing synergy with classical optical networks, with the ability to support many qubits in a single fiber. Yet, coherent quantum frequency operations prove extremely challenging due to the difficulties in mixing frequencies arbitrarily and with low noise. In this paper, we address such challenges and implement distinct quantum gates in parallel on two entangled frequency-bin qubits in the same optical fiber. Our basic quantum operation controls the spectral overlap between adjacent spectral bins, allowing us to observe frequency-bin Hong–Ou–Mandel interference with a visibility of 0.971 ± 0.007. By integrating this tunability with frequency parallelization, we synthesize independent gates on entangled qubits and flip their spectral correlations, allowing us to observe strong violation of the separability bound. Our realization of closed, user-defined gates on frequency-bin qubits in parallel should find application in the development of fiber-compatible quantum information processing and quantum networks.

https://doi.org/10.1364/OPTICA.5.001455

1. INTRODUCTION

Quantum information encoding in optical frequency offers an intriguing possibility for quantum computing both on chip and over distributed fiber networks. Considerable progress has been made in generating two-photon entanglement across a comb of narrowband frequency modes, or bins, including optical parametric oscillators below threshold [1], filtering of broadband parametric downconversion [2], and, recently, on-chip production of quantum frequency combs using microring resonators [3–6]. Likewise, research in quantum frequency conversion has showcased coherent translation of single-photon states across both wide [7,8] and narrow [9] bandwidths.

Moving beyond entangled-state production and single-photon frequency manipulation to full-fledged quantum information processing in frequency-encoded qubits, a crucial experimental capability is missing. First and foremost, one must be able to apply independent and distinct gates efficiently and with low noise to multiple qubits on demand. In this paper, we demonstrate that tunable and independent single-frequency-qubit operations can be implemented in parallel on co-propagating qubits. Specifically, we realize a qubit operation that can be tuned smoothly between the identity $\mathbb{1}$ and Hadamard H gates and that can realize any combination thereof in parallel in the same device. We characterize this operation's tunability with frequency-bin Hong–Ou–Mandel (HOM) interference, obtaining 97% visibility for distinct frequency bins, the highest yet observed for photons of different colors. We then implement this operation as two separate quantum gates on frequency-bin qubits within the same fiber-optic mode, obtaining a high-fidelity flip of spectral correlations on two entangled photons. Our results demonstrate multiple functionalities in parallel in a single platform, representing an important step forward for quantum information processing in the frequency domain.

2. BACKGROUND

Interest in frequency-based photonic quantum information processing has grown significantly in recent years. When selected properly, the frequency degree of freedom is compatible with optical fiber and valuable for scaling up quantum memories [10], and potentially large amounts of information can be stored in single photons in spectro-temporal modes [11–14]. Yet, while frequency multiplexing is fairly straightforward in the quantum domain, universal quantum gate sets in frequency space are much more challenging to implement. As important milestones, frequency beamsplitters, based either on optical nonlinearities [15–17] or electro-optic modulation [18,19], have shown

coherent interference of frequency-encoded photons, and quantum pulse gates [12,20–23] based on mixing single photons with shaped control fields have allowed state discrimination of orthogonal time-frequency pulsed modes. Yet, the ability to perform distinct and controlled operations simultaneously across several qubits in the same spatial mode has thus far remained elusive. Nonlinear-optics-based approaches offer such a capability in theory by using multiple strong pump fields. However, the prospects of scaling such approaches with low noise to two or more qubits are uncertain. Alternatively, a fully linear-optic scheme for quantum information processing with time-bin encoding has also been developed [24]. While in principle enabling universal quantum computing in a single spatial mode, its requirement of fast polarization rotation—or alternatively, long birefringent delay—makes it challenging to realize in its pure, single-spatial-mode form. Indeed, the seminal experimental implementation enlisted ancillary spatial modes for time/polarization conversion, so a fully single-spatial-mode realization is still missing [24]. Finally, in the case of frequency-bin encoding, electro-optic approaches such as the one we pursue here excel at performing the same low-noise quantum gate on multiple qubits in parallel but so far have been unable to perform different gates concurrently.

Yet, of the frequency-bin processing approaches available, the combination of electro-optic phase modulators (EOMs) and Fourier transform pulse shapers [25] seems well suited for removing this limitation and scaling up frequency-based quantum networks. This paradigm is sufficient for universal quantum computing, requires no optical pump fields, has low noise, and accepts broadband inputs without the need for tailored phase matching [18,26]. Even more importantly, the fact that pulse shapers apply arbitrary phase shifts to each frequency mode suggests the possibility of synthesizing *different* frequency-bin gates on two qubits in parallel, even when they experience the *same* temporal modulation from the EOMs. As we demonstrate in the following, this intuition is indeed correct; by adjusting only spectral phase, we can realize fully controlled and independent operations in parallel on spectrally separated qubits.

3. CONCEPT OF OPERATION

Figure 1 sketches an example of how such principles could be applied in a parallel frequency processor, with the particular operations chosen to match the experiments in this paper. In general, an input quantum state consisting of frequency-encoded qubits is manipulated by the designed network of EOMs and pulse shapers, which applies various unitary operations to combinations of frequency bins. Conceptually, each EOM serves as a frequency mode mixer, while the specific phase patterns applied by each pulse shaper enable either constructive or destructive interference in different frequency bins at the subsequent EOM. The use of EOMs and pulse shapers is thus analogous to the beamsplitters and variable retarders in spatial/polarization optical multiports, with the key difference being that while the standard spatial approach builds on two-mode beamsplitters, each EOM interferes all modes simultaneously. Therefore, a more precise spatial equivalent to each EOM would be a multimode coupler instead of a beamsplitter. Finally, as in the spatial case, feed-forward operations are compatible here as well; after each step in the quantum frequency processor, a subset of modes could be extracted with optical add-drop multiplexers and measured, with the results used to update operations downstream. Note that, although

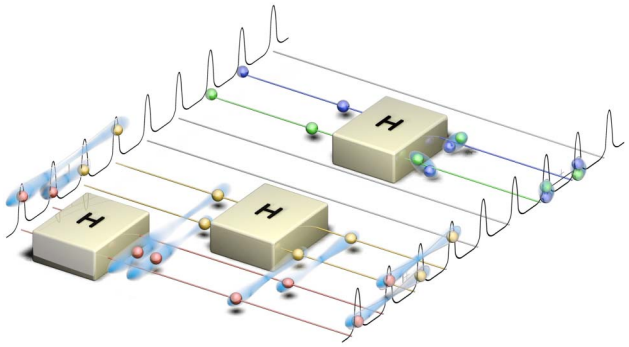

Fig. 1. High-level vision of quantum frequency processor. Single photons (spheres) populating a comb of frequency bins propagate through a parallelized network of quantum gates (boxes) performing the desired set of operations. Spheres of a specific color trace the probability amplitudes of a single input photon, so that an ideal measurement will register precisely one click for each color. Frequency superpositions are represented by spheres straddling multiple lines, while entangled states are sums of photon products (visualized by clouds containing spheres of the same pair of colors). The specific operations are those we realize experimentally: HOM interference (top) and parallel single-qubit rotations (bottom).

we draw each frequency bin as a separate "rail" for conceptual purposes, the physical encoding occurs within a single fiber-optic spatial mode, thereby enabling natural phase stability and providing compatibility with current fiber networks. This vision is considerably more broad than our previous experiments on frequency beamsplitters and tritters [18], for it exploits quantum entanglement (i.e., nonclassical two-qubit, rather than just single-qubit, effects) and realizes different operations in the same device simultaneously, rather than the *same* operation in parallel over many modes—a valuable, though less general, form of parallelizability [18].

Any pair of distinct quantum gates that can be implemented in parallel in our approach must satisfy two requirements: (i) their physical implementations must differ only in the spectral phase applied by each, since the temporal modulation is shared by all frequency-bin gates in a single spatial mode, and (ii) they must be able to be realized independently in two frequency bands without crosstalk. These considerations are general, holding for any proposed set of parallel gates. Yet in the particular example we consider here, a tunable frequency beamsplitter, we can connect these two requirements directly to nonclassical phenomena of particular significance in quantum photonics: HOM interference [27] and the Einstein–Podolsky–Rosen (EPR) paradox [28].

In the conventional HOM interferometer, two photons mixed on a 50/50 spatial beamsplitter bunch, never exiting in different output ports. A general feature of bosons, HOM interference forms the basis of essentially all two-qubit gates in linear optics [29]. In our case, the overlap between frequency bins is set by the spectral phase of the quantum frequency processor, so that HOM interference relies precisely on the ability to tune a given operation through spectral phase control alone; in other words, high visibility provides confirmation of requirement (i) above. Similarly, quantum mechanics allows two particles to share a well-defined pure state, even when the individual states of both particles are mixed. This property gives rise to EPR correlations when the joint state of the two particles is measured. While paradoxical to classical notions of reality [28], these correlations ultimately

underpin Bell tests of nonlocality [30] and security in quantum key distribution [31]. Meeting requirement (ii) above signifies the ability to perform independent gates on entangled frequency-bin qubits. In particular, joint beamsplitter operations with different phases enable the realization of all combinations of Pauli Z and X basis measurements, which are sufficient for testing EPR correlations. Consequently, in the following experiments we utilize both quantum phenomena (HOM and EPR) as important test cases to assess gate performance.

4. EXPERIMENTAL RESULTS

Figure 2(a) shows our setup for processing quantum information encoded in frequency. Our test source of entanglement is a biphoton frequency comb (BFC) generated by pumping a periodically poled lithium niobate (PPLN) waveguide with a continuous-wave Ti:sapphire laser and filtering the broadband emission with an etalon to produce frequency bins. The resulting state is of the form $|\Psi\rangle = \sum_{n\geq 1} c_n |1_{\omega_{1-n}}\rangle_A |1_{\omega_n}\rangle_B$, where the coefficients c_n are set by a pulse shaper (BFC shaper). Each frequency-bin index n corresponds to the filter centered at $\omega_n = \omega_0 + n\Delta\omega$, where $\omega_0/2\pi = 193.6000$ THz (International Telecommunication Union channel 36 at 1548.51 nm) and $\Delta\omega/2\pi = 25$ GHz. Party A is assigned all modes $n_A \in \{n \leq 0\}$, while the rest are given to B ($n_B \in \{n \geq 1\}$). In Fig. 2(b), we plot the measured frequency correlations of this source, obtained by bypassing the quantum frequency processor (QFP), scanning the filters of the output wavelength-selective switch, and counting coincidences between two detectors. Over this 50×50 mode grid, we observe high coincidence counts only for frequency-bin pairs satisfying $n_A + n_B = 1$, as expected by energy conservation. The processor itself consists of a pulse shaper sandwiched between two EOMs. Each EOM is driven by a 25 GHz sinusoidal voltage, while the pulse shaper imparts a user-defined phase to each spectral bin; this combination was shown to enable a frequency Hadamard gate H with 99.998% fidelity and only 2.61% photon leakage into neighboring modes [18].

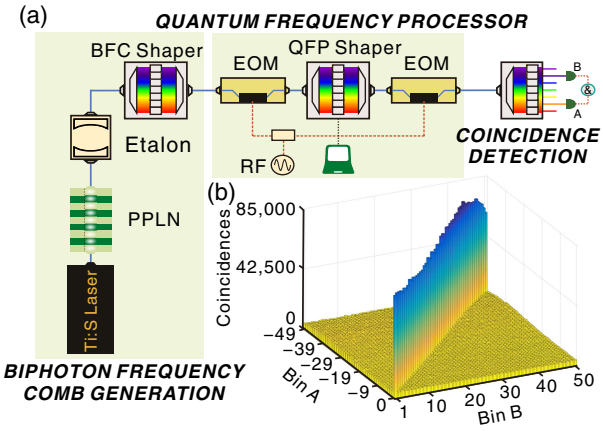

Fig. 2. (a) Experimental configuration. (b) Joint frequency spectrum of source, measured with etalon output connected directly to coincidence detection setup. Frequency bins satisfying $n_A + n_B = 1$ show strong correlations, whereas all other combinations are at the expected accidentals level. Coincidences are counted over 5 s.

By modifying the spectral phase applied by this H gate, or frequency-bin beamsplitter, we can realize the desired tunable quantum operation forming the basis for distinct parallel gates. As we have discovered, changing the depth of the phase shift imparted by the pulse shaper between frequency bins 0 and 1 allows the spectral reflectivity $\mathcal{R}$ to be tuned smoothly from 0 to ~0.5 and back to 0; see Supplement 1 for details. Figure 3(a) plots the theoretically predicted (curves) and experimentally measured (symbols) beamsplitter transmission and reflection coefficients between bins 0 and 1, when probing the system with a laser and scanning the shaper phase. A phase setting of π results in an H gate; 0 and 2π phase shifts yield an identity operation. It is important to emphasize that both EOMs remain fixed throughout the scan, so that the tunability is effected only by adjusting the phase applied by the pulse shaper. This controlled reflectivity can be tested directly on quantum states via HOM interference. In general for HOM, one must scan some parameter that controls the distinguishability of the two-photon probability amplitudes leading to clicks on both output detectors; a visibility exceeding 50% indicates nonclassicality [27]. In the case of photons of different colors, this interference can be realized with a frequency mixer [15] where, e.g., the distinguishability is controlled by introducing a temporal delay between the two input modes [16] or scanning the photon frequency spacing relative to that of the frequency beamsplitter [19,32]. Here we adjust the mixing probability of the operation itself, as controlled by the phase scanned in Fig. 3(a), analogous to varying the reflectivity of a spatial beamsplitter.

Sending in the photon pair $|1_{\omega_0}\rangle_A |1_{\omega_1}\rangle_B$ and scanning the QFP pulse shaper phase, we measure the coincidence counts between output bins 0 and 1 shown in Fig. 3(b). The solid curve is the theoretical prediction, scaled and vertically offset to match

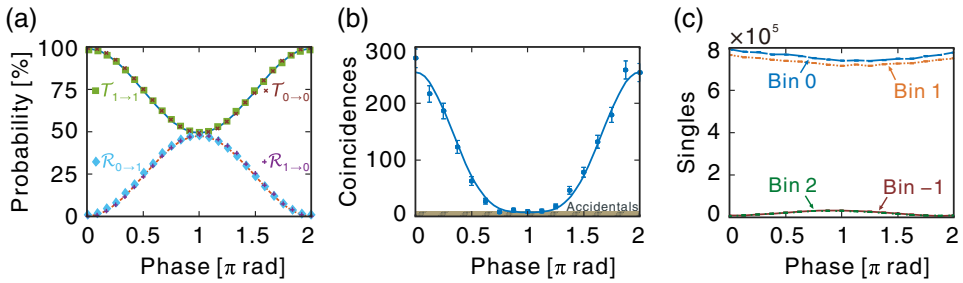

Fig. 3. (a) Beamsplitter reflectivities $\mathcal{R}$ and transmissivities $\mathcal{T}$ for all paths between frequency bins 0 and 1, as pulse shaper phase shift is tuned. Markers denote the values measured with a laser probe, while curves give the theory. (b) Measured output coincidence counts between bins 0 and 1, for a two-photon input (no accidentals subtraction). The HOM visibility is 0.971 ± 0.007. (c) Singles counts in bins 0, 1, −1, and 2 for the same input as (b). Here, detector dark counts are subtracted to compare output flux. For (b) and (c), counts are recorded over 180 s, and error bars assume Poissonian statistics.

the data points via linear least squares; the visibility obtained from this fit is 0.971 ± 0.007, with the reduction from unity completely consistent with the accidentals level expected for our measured counts and timing resolution. This visibility far exceeds the previous values measured for frequency-domain HOM interference without subtraction of accidentals [33]—namely, 0.71 ± 0.04 [16] and 0.68 ± 0.03 [32]. Such a significant improvement in visibility can be explained by the reduced optical noise present in our electro-optic-based approach, compared to those relying on powerful pump fields, as well as the fine controllability of our operation, enabled by the purely electrical control parameters (i.e., microwave power, microwave phase, and pixel voltages for the pulse shaper), which allows us to precisely optimize the spectral overlap between the two modes.

We also record the singles counts for bins 0 and 1, as well as the adjacent sidebands (−1 and 2). As shown in Fig. 3(c), the two central modes retain nearly constant flux across the full scan, showing that the dip in coincidence counts results from truly quantum HOM interference as opposed to photon loss; see Supplement 1 for a further discussion on this point. Moreover, the small reduction in singles counts around π—accompanied by the increase in singles counts for bins −1 and 2—also qualitatively matches expectations, given the fact that the full H gate scatters 2.61% of the input photons out of the computational space into adjacent sidebands. We note that even this scattering could be removed by driving the EOMs with more complicated waveforms [26]. Indeed, the deterministic nature of our tunable frequency beamsplitter sets this HOM experiment apart from alternatives using a single EOM, which can only overlap adjacent bins *probabilistically*, due to higher-order scattering into sideband modes [19]. While perfectly acceptable for HOM interference *per se*, such extra scattering proves inadequate for our goal here—general-purpose quantum information processing—where HOM interference serves as a building block within larger linear-optical gates. In this context, limiting scattering into extraneous frequency bins is critical to facilitate high success probability.

Our quantum operation's tunability, invoked in the above realization of HOM interference, can then be applied to realize two different gates—that is, distinct pairs of $\mathcal{R}$ and $\mathcal{T}$ in Fig. 3(a)—by setting different phase shifts on appropriate subbands in the pulse shaper's bandwidth. To demonstrate this, we set the BFC shaper to pass modes $\{-4, -3, 4, 5\}$ [cf. Fig. 2(b)], preparing the input entangled state $|\Psi\rangle \propto |1_{\omega_{-4}}\rangle_A |1_{\omega_5}\rangle_B + |1_{\omega_{-3}}\rangle_A |1_{\omega_4}\rangle_B$. On each pair of frequency bins—$\{-4, -3\}$ and $\{4, 5\}$—we set the spectral phase to apply either the identity $\mathbb{1}$ or Hadamard H gates and then measure coincidence counts between the frequency bins at the output. Figure 4 furnishes the results for all four combinations of $\mathbb{1}$ and H. When the two gates match, near-perfect spectral correlations result [Figs. 4(a) and 4(d)], whereas mismatched cases produce uniform population of the two-qubit space [Figs. 4(b) and 4(c)]. By measuring correlations in adjacent bins as well, we confirm the self-contained nature of our operation; even in the worst case [Fig. 4(d)], less than 6% of the total coincidences lie outside of the 2×2 subspace, whereas similar state manipulation with only one EOM suffers from high probability of qubit scattering [5,6,19]. The loss of photon energy to unwanted sideband modes is intrinsic to frequency-bin operations based on a single EOM (see discussion in Ref. [18]). Thus, they are inherently nondeterministic and can be viewed at best only as postselected single-photon gates.

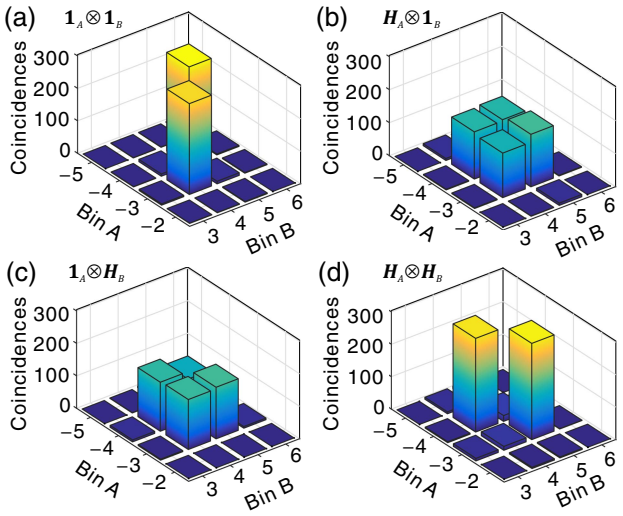

Fig. 4. Coincidences between output frequency bins after the following gates: (a) $\mathbb{1}$ on both photons, (b) H on photon A, (c) H on photon B, (d) H on both photons. Coincidences are collected over 120 s.

While sufficient for the projective-type measurements required in, e.g., state tomography and Bell-inequality tests [5,6], such frequency-bin operations cannot be classified as gates in the sense of performing coherent rotations within a fixed input/output Hilbert space. By contrast, the manipulations shown in Fig. 4 do represent frequency-bin gates in this proper sense, and thus offer potential in constructing more general quantum information processing networks. In particular, because our frequency-bin operations retain photons in their respective computational spaces, they can be concatenated in systems containing several successive gates, without the massive reduction in success probability inherent to previous approaches.

Importantly, we note that the transition from $\mathbb{1}_A \otimes \mathbb{1}_B$ [Fig. 4(a)] to $H_A \otimes H_B$ [Fig. 4(d)] actually flips the correlations entirely, eliminating the negative frequency dependence resulting from pump energy conservation in favor of a positive dependence. Similar conversion of spectral correlation has been demonstrated for continuous frequency-entangled photons, via nonlinear mixing with a tailored optical pump pulse [34]. In our example, we show how the frequency entanglement in discrete bins can be likewise manipulated, now with an electro-optic-based approach. This demonstration of two single-qubit rotations that are closed in the four-dimensional frequency-bin computational space is essential for the ideal two-level logic underpinning qubit-based forms of quantum information processing.

And so, looking toward prospects for scaling up our parallel gates, we note that extension in the frequency dimension is straightforward; just as we have realized identical frequency beamsplitters over the entire optical C-band [18], one should be able to synthesize these more general operations over the full ∼40 nm pulse shaper bandwidth with negligible reduction in fidelity. Similarly, extending from qubit to higher-dimensional qudit encoding is possible too, in which more general $d \times d$ frequency-bin gates can be constructed by the same EOM–pulse shaper–EOM setup, but with microwave drive signals consisting of $d - 1$ single-frequency harmonics [18]. Admittedly, synthesizing many such harmonics places strong demands on the required EOM bandwidth, which at present poses practical challenges for

experimental implementation. This situation suggests that incorporating nonlinear optical mixers as well may be useful to bridge frequency gaps too wide for state-of-the-art modulators; the intersection of electro-optics and nonlinear optics in the context of quantum information processing thus appears an interesting direction for further research.

5. BAYESIAN STATE ANALYSIS

The quality of our state manipulation can be analyzed by equivalently viewing the unitary *rotations* on our input state followed by coincidence detection as *measurements* of the state in bases other than computational. As one example, we can test the EPR-like nature of this state using the strong correlations in two mutually unbiased bases Z and X (gate operations $\mathbb{1}$ and H). We define the conditional entropies $\mathcal{H}(\mathbb{1}_A|\mathbb{1}_B)$ and $\mathcal{H}(H_A|H_B)$ as the uncertainty of the measured frequency mode of A $\{-4, -3\}$ given knowledge of B's result $\{4, 5\}$ for the two cases of matched transformations [Figs. 4(a) and 4(d)]. Retrieving the probabilities from the raw counts via Bayesian mean estimation (BME) with no accidentals subtraction, we recover $\mathcal{H}(\mathbb{1}_A|\mathbb{1}_B) = 0.19 \pm 0.03$ and $\mathcal{H}(H_A|H_B) = 0.29 \pm 0.04$. The entanglement can be quantified by violation of the Maassen–Uffink bound for separable states: $\mathcal{H}(\mathbb{1}_A|\mathbb{1}_B) + \mathcal{H}(H_A|H_B) \geq q_{\mathrm{MU}}$ [35,36]. In our case, the bound q_{MU} is computed to be 0.971, just smaller than 1 because of slight imbalance in our H operation (see Supplement 1 for details). With the sum, $\mathcal{H}(\mathbb{1}_A|\mathbb{1}_B) + \mathcal{H}(H_A|H_B) = 0.48 \pm 0.05$, we thus violate the q_{MU} bound by 9.8 standard deviations, providing a clear witness of entanglement in our system.

Moreover, BME allows us to estimate the full density matrix from just the four measurements in Fig. 4, with any missing tomographic information reflected naturally in the retrieved uncertainty [37,38]. The operations above—$\mathbb{1}$ and H followed by frequency-bin detection—are equivalent to measurements in the Pauli Z and X bases, respectively. Using this information, BME produces the density matrix $\hat{\rho}$ in Fig. 5: the mean values of the real and imaginary components are plotted in Figs. 5(a) and 5(b); their associated standard deviations are shown in Figs. 5(c) and 5(d) (see Supplement 1 for model details). The power of Bayesian inference is particularly evident in the error. It is extremely low for the real elements, due to our complete coverage of the Z and X bases, yet much larger on several of the imaginary components, as expected given the absence of results in the Pauli Y basis. Since physical requirements do bound this error, we can still strongly bound our estimate of the fidelity compared to the ideal state $|\Psi^+\rangle \propto |1_{\omega_{-4}}\rangle_A|1_{\omega_5}\rangle_B + |1_{\omega_{-3}}\rangle_A|1_{\omega_4}\rangle_B$. Specifically, the Bayesian estimate is $\mathcal{F} = \langle\Psi^+|\hat{\rho}|\Psi^+\rangle = 0.92 \pm 0.01$. This result provides positive corroboration of our frequency-bin control and is fairly conservative, given that: (i) dark counts are not removed and thus can degrade the state, and (ii) we intentionally lump any imperfections in our system onto the state itself, so that impurities in either the input state or quantum frequency processor will contribute to a lower $\mathcal{F}$. Such findings demonstrate the utility of our quantum frequency processor for manipulating joint quantum systems coherently and independently, preserving a state's built-in entanglement in the process—an essential functionality in frequency-bin qubit control.

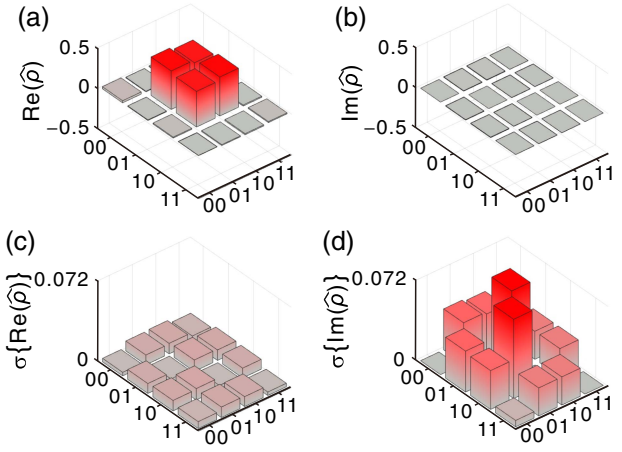

Fig. 5. Density matrix retrieved by BME. (a) Real part of average density matrix. (b) Imaginary part. (c) Standard deviations of the real density matrix elements. (d) Standard deviations of the imaginary elements. Shorthand label definitions: $00 \equiv |1_{\omega_{-4}}\rangle_A|1_{\omega_4}\rangle_B$, $01 \equiv |1_{\omega_{-4}}\rangle_A|1_{\omega_5}\rangle_B$, $10 \equiv |1_{\omega_{-3}}\rangle_A|1_{\omega_4}\rangle_B$, $11 \equiv |1_{\omega_{-3}}\rangle_A|1_{\omega_5}\rangle_B$.

Funding. Laboratory Directed Research and Development Program of Oak Ridge National Laboratory (ORNL) managed by UT-Battelle, LLC, for the U.S. Department of Energy (DEAC05-00OR22725).

Acknowledgment. Portions of this work were presented at CLEO 2018 as paper number JTh5B.3. We thank A. Sproles for the graphics in Fig. 1, D. E. Leaird for technical assistance, and B. Qi for valuable discussions.

See Supplement 1 for supporting content.

†These authors contributed equally for this work.

REFERENCES AND NOTES

1. Y. J. Lu, R. L. Campbell, and Z. Y. Ou, "Mode-locked two-photon states," Phys. Rev. Lett. **91**, 163602 (2003).
2. Z. Xie, T. Zhong, S. Shrestha, X. Xu, J. Liang, Y.-X. Gong, J. C. Bienfang, A. Restelli, J. H. Shapiro, F. N. C. Wong, and C. W. Wong, "Harnessing high-dimensional hyperentanglement through a biphoton frequency comb," Nat. Photonics **9**, 536–542 (2015).
3. C. Reimer, M. Kues, P. Roztocki, B. Wetzel, F. Grazioso, B. E. Little, S. T. Chu, T. Johnston, Y. Bromberg, L. Caspani, D. J. Moss, and R. Morandotti, "Generation of multiphoton entangled quantum states by means of integrated frequency combs," Science **351**, 1176–1180 (2016).
4. J. A. Jaramillo-Villegas, P. Imany, O. D. Odele, D. E. Leaird, Z.-Y. Ou, M. Qi, and A. M. Weiner, "Persistent energy-time entanglement covering multiple resonances of an on-chip biphoton frequency comb," Optica **4**, 655–658 (2017).
5. M. Kues, C. Reimer, P. Roztocki, L. R. Cortés, S. Sciara, B. Wetzel, Y. Zhang, A. Cino, S. T. Chu, B. E. Little, D. J. Moss, L. Caspani, J. Azaña, and R. Morandotti, "On-chip generation of high-dimensional entangled quantum states and their coherent control," Nature **546**, 622–626 (2017).
6. P. Imany, J. A. Jaramillo-Villegas, O. D. Odele, K. Han, D. E. Leaird, J. M. Lukens, P. Lougovski, M. Qi, and A. M. Weiner, "50-GHz-spaced comb of high-dimensional frequency-bin entangled photons from an on-chip silicon nitride microresonator," Opt. Express **26**, 1825–1840 (2018).
7. J. Huang and P. Kumar, "Observation of quantum frequency conversion," Phys. Rev. Lett. **68**, 2153–2156 (1992).
8. S. Tanzilli, W. Tittel, M. Halder, O. Alibart, P. Baldi, N. Gisin, and H. Zbinden, "A photonic quantum information interface," Nature **437**, 116–120 (2005).

9. L. J. Wright, M. Karpiński, C. Söller, and B. J. Smith, "Spectral shearing of quantum light pulses by electro-optic phase modulation," Phys. Rev. Lett. **118**, 023601 (2017).
10. N. Sinclair, E. Saglamyurek, H. Mallahzadeh, J. A. Slater, M. George, R. Ricken, M. P. Hedges, D. Oblak, C. Simon, W. Sohler, and W. Tittel, "Spectral multiplexing for scalable quantum photonics using an atomic frequency comb quantum memory and feed-forward control," Phys. Rev. Lett. **113**, 053603 (2014).
11. J. M. Lukens, A. Dezfooliyan, C. Langrock, M. M. Fejer, D. E. Leaird, and A. M. Weiner, "Orthogonal spectral coding of entangled photons," Phys. Rev. Lett. **112**, 133602 (2014).
12. B. Brecht, D. V. Reddy, C. Silberhorn, and M. G. Raymer, "Photon temporal modes: a complete framework for quantum information science," Phys. Rev. X **5**, 041017 (2015).
13. T. Zhong, H. Zhou, R. D. Horansky, C. Lee, V. B. Verma, A. E. Lita, A. Restelli, J. C. Bienfang, R. P. Mirin, T. Gerrits, S. W. Nam, F. Marsili, M. D. Shaw, Z. Zhang, L. Wang, D. Englund, G. W. Wornell, J. H. Shapiro, and F. N. C. Wong, "Photon-efficient quantum key distribution using time-energy entanglement with high-dimensional encoding," New J. Phys. **17**, 022002 (2015).
14. N. T. Islam, C. C. W. Lim, C. Cahall, J. Kim, and D. J. Gauthier, "Provably secure and high-rate quantum key distribution with time-bin qudits," Sci. Adv. **3**, e1701491 (2017).
15. M. Raymer, S. van Enk, C. McKinstrie, and H. McGuinness, "Interference of two photons of different color," Opt. Commun. **283**, 747–752 (2010).
16. T. Kobayashi, R. Ikuta, S. Yasui, S. Miki, T. Yamashita, H. Terai, T. Yamamoto, M. Koashi, and N. Imoto, "Frequency-domain Hong-Ou–Mandel interference," Nat. Photonics **10**, 441–444 (2016).
17. S. Clemmen, A. Farsi, S. Ramelow, and A. L. Gaeta, "Ramsey interference with single photons," Phys. Rev. Lett. **117**, 223601 (2016).
18. H.-H. Lu, J. M. Lukens, N. A. Peters, O. D. Odele, D. E. Leaird, A. M. Weiner, and P. Lougovski, "Electro-optic frequency beam splitters and tritters for high-fidelity photonic quantum information processing," Phys. Rev. Lett. **120**, 030502 (2018).
19. P. Imany, O. D. Odele, M. S. Alshaykh, H.-H. Lu, D. E. Leaird, and A. M. Weiner, "Frequency-domain Hong-Ou-Mandel interference with linear optics," Opt. Lett. **43**, 2760–2763 (2018).
20. V. Ansari, J. M. Donohue, M. Allgaier, L. Sansoni, B. Brecht, J. Roslund, N. Treps, G. Harder, and C. Silberhorn, "Tomography and purification of the temporal-mode structure of quantum light," Phys. Rev. Lett. **120**, 213601 (2018).
21. P. Manurkar, N. Jain, M. Silver, Y.-P. Huang, C. Langrock, M. M. Fejer, P. Kumar, and G. S. Kanter, "Multidimensional mode-separable frequency conversion for high-speed quantum communication," Optica **3**, 1300–1307 (2016).
22. D. V. Reddy and M. G. Raymer, "High-selectivity quantum pulse gating of photonic temporal modes using all-optical Ramsey interferometry," Optica **5**, 423–428 (2018).
23. V. Ansari, J. M. Donohue, B. Brecht, and C. Silberhorn, "Tailoring nonlinear processes for quantum optics with pulsed temporal-mode encodings," Optica **5**, 534–550 (2018).
24. P. C. Humphreys, B. J. Metcalf, J. B. Spring, M. Moore, X.-M. Jin, M. Barbieri, W. S. Kolthammer, and I. A. Walmsley, "Linear optical quantum computing in a single spatial mode," Phys. Rev. Lett. **111**, 150501 (2013).
25. A. M. Weiner, "Ultrafast optical pulse shaping: a tutorial review," Opt. Commun. **284**, 3669–3692 (2011).
26. J. M. Lukens and P. Lougovski, "Frequency-encoded photonic qubits for scalable quantum information processing," Optica **4**, 8–16 (2017).
27. C. K. Hong, Z. Y. Ou, and L. Mandel, "Measurement of subpicosecond time intervals between two photons by interference," Phys. Rev. Lett. **59**, 2044–2046 (1987).
28. A. Einstein, B. Podolsky, and N. Rosen, "Can quantum-mechanical description of physical reality be considered complete?" Phys. Rev. **47**, 777–780 (1935).
29. P. Kok, W. J. Munro, K. Nemoto, T. C. Ralph, J. P. Dowling, and G. J. Milburn, "Linear optical quantum computing with photonic qubits," Rev. Mod. Phys. **79**, 135–174 (2007).
30. J. S. Bell, "On the Einstein Poldolsky Rosen paradox," Physics Physique Fizika **1**, 195–200 (1964).
31. N. Gisin, G. Ribordy, W. Tittel, and H. Zbinden, "Quantum cryptography," Rev. Mod. Phys. **74**, 145–195 (2002).
32. C. Joshi, A. Farsi, and A. Gaeta, "Hong–Ou–Mandel interference in the frequency domain," in *Conference on Lasers and Electro-Optics (CLEO)* (Optical Society of America, 2017), paper FF2E.3.
33. We note that, due to low signal-to-noise ratios, the experiment in Ref. [19] required subtraction of accidental coincidences to exceed the classical limit, so we do not include its 84% visibility in the comparison in the main text. Incidentally, if we subtract accidentals from the present results [Fig. 3(b)], the visibility will increase to $\sim 100\%$.
34. J. M. Donohue, M. Mastrovich, and K. J. Resch, "Spectrally engineering photonic entanglement with a time lens," Phys. Rev. Lett. **117**, 243602 (2016).
35. H. Maassen and J. B. M. Uffink, "Generalized entropic uncertainty relations," Phys. Rev. Lett. **60**, 1103–1106 (1988).
36. P. J. Coles, M. Berta, M. Tomamichel, and S. Wehner, "Entropic uncertainty relations and their applications," Rev. Mod. Phys. **89**, 015002 (2017).
37. R. Blume-Kohout, "Optimal, reliable estimation of quantum states," New J. Phys. **12**, 043034 (2010).
38. B. P. Williams and P. Lougovski, "Quantum state estimation when qubits are lost: a no-data-left-behind approach," New J. Phys. **19**, 043003 (2017).